

Uranium In Situ Electrolytic Deposition with a Reusable Functional Graphene-Foam Electrode

Chao Wang,* Ahmed S. Helal, Ziqiang Wang, Jian Zhou, Xiahui Yao, Zhe Shi, Yang Ren, Jinhyuk Lee, Jeng-Kuei Chang, Bunshi Fugetsu, and Ju Li*

Nuclear fission produces 400 GWe which represents 11% of the global electricity output. Uranium is the essential element as both fission fuel and radioactive waste. Therefore, the recovery of uranium is of great importance. Here, an in situ electrolytic deposition method to extract uranium from aqueous solution is reported. A functionalized reduced graphene oxide foam (3D-FrGOF) is used as the working electrode, which acts as both a hydrogen evolution reaction catalyst and a uranium deposition substrate. The specific electrolytic deposition capacity for U(VI) ions with the 3D-FrGOF is 4560 mg g⁻¹ without reaching saturation, and the Coulombic efficiency can reach 54%. Moreover, reduction of the uranium concentration in spiked seawater from 3 ppm to 19.9 ppb is achieved, which is lower than the US Environmental Protection Agency uranium limits for drinking water (30 ppb). Furthermore, the collection electrode can be efficiently regenerated and recycled at least nine times without much efficiency fading, by ejecting into 2000 ppm concentrated uranium solution in a second bath with reverse voltage bias. All these findings open new opportunities in using free-standing 3D-FrGOF electrode as an advanced separation technique for water treatment.

of the radioactive by-product and spent nuclear fuel that has long-term radioactivity. According to Environmental Protection Agency (EPA), drinking water contaminated with uranium concentration higher than 0.03 mg L⁻¹ (30 ppb) can lead to serious health effects such as kidney damage, cancer risk, and neurobehavioral changes. Hence, efficient extraction of uranium from mining and contaminated water solutions is vital for the environment and public health as well as the reuse of uranium resources.^[3]

Various methods have been developed to extract uranium from mining and contaminated water. Ion exchange is the most widely used technique to remove uranium. The drawbacks of ion exchange resins are poor selectivity, low adsorption capacity, incomplete removal of uranyl ions and problematic disposal of spent ion exchange resins.^[4] Membrane methods that include reverse osmosis and nano-

filtration have been used to remove uranium, with relatively larger size of uranium compounds than the pore of the membranes. This method is effective, but it is expensive and most of the membranes are not reusable.^[5] For large-scale water treatment plants, alum coagulation and lime softening methods can be used. However, these two methods suffer from low removal efficiency and work under strongly alkaline conditions.^[6] The electrochemical deposition method is an effective way to extract


1. Introduction

Nuclear energy is a known solution to the global energy problem, offering high energy density and low greenhouse gas emissions.^[1] There are 442 nuclear power plants around the world, and 60 more new nuclear plants are under construction. Most of the nuclear fission reactors use uranium (U) as fission fuel.^[2] Uranium also accounts for a high proportion

Dr. C. Wang, Dr. A. S. Helal, Dr. Z. Wang, Prof. J. Zhou, Dr. X. Yao,
Dr. Z. Shi, Prof. J. Lee, Prof. J. Li
Department of Nuclear Science and Engineering
Massachusetts Institute of Technology
Cambridge, MA 02139, USA
E-mail: chaow@mit.edu; liju@mit.edu

Dr. C. Wang
School of Materials Science and Engineering
Tongji University
Shanghai 201804, China

Dr. A. S. Helal
Nuclear Materials Authority
P.O. Box 540, El Maadi, Cairo, Egypt

 The ORCID identification number(s) for the author(s) of this article can be found under <https://doi.org/10.1002/adma.202102633>.

Dr. Y. Ren
Advanced Photon Source
Argonne National Laboratory
9700 South Cass Avenue, Lemont, IL 60439, USA

Prof. J.-K. Chang
Department of Materials Science and Engineering
National Chiao Tung University
Hsinchu 30010, Taiwan

Prof. B. Fugetsu
Institute for Future Initiatives
The University of Tokyo
Bunkyo-ku, Tokyo 113-0032, Japan

Prof. J. Li
Department of Materials Science and Engineering
Massachusetts Institute of Technology
Cambridge, MA 02139, USA

DOI: 10.1002/adma.202102633

uranium. Xu et al. reported a carbon fiber electrode that can deposit uranium efficiently with a capacity of 1200 mg g⁻¹. Liu et al. developed a half-wave rectified alternating current electrochemical method with a uranium extraction capacity of 1932 mg g⁻¹ using an amidoxime-functionalized carbon electrode.^[7] But their Coulombic efficiency needs further improvement, and the ejection into high concentration disposal was not demonstrated. The development of an efficient and reusable uranium deposition electrode would be advantageous.

The objective of our research is to develop an efficient and sustainable extraction method for uranium from polluted industrial wastewater (high U concentration, on the order of many ppm) and drinking water (low U concentration, on the order of the EPA limit of 30 ppb) through an electrolytic process, that can work robustly despite interference from other ions in the water (e.g., seawater-like solution) and achieve below 30 ppb(U) outcome in order for the water to be drinkable. Guided by the uranium Pourbaix diagram and water splitting phenomenon, we propose to use hydrogen evolution reaction (HER) to increase the local pH of the electrode, then the uranium cations that move to the working electrode under electric field will be induced to deposit out of the solution and grafted onto the electrode. The working electrode has the ability to catalyze HER to decrease the overpotential and increase the degree of local pH increase. The local pH increase is necessary to produce the bridging hydroxy anions on the electrode surface, which can induce polymerization of uranyl cations and deposition of a charge-neutral uranium polymer. The choice of a suitable HER catalyst working electrode is essential. Here, a 3D functional reduced graphene oxide foam (3D-FrGOF) was doped and modified with several elemental and functional groups. It was then used as the working electrode in electrolytic deposition. The use of a 3D-FrGOF electrode can benefit from its large surface area and flexible functionalizations, which can both promote HER and uranium deposition. Elemental doping of sulfur and nitrogen are essential for the complexation with uranium ions to form the initial crystallization site for uranium deposition. The electronic conductivity of 3D-FrGOF is good and can be used as a free-standing electrode directly.

This in situ electrolytic deposition method is simple, efficient, and clean; no extra chemical pollution will be introduced. We have achieved a uranium extraction capacity of 4560 mg g⁻¹ using 3D-FrGOF electrode, without observing capacity saturation. The Coulombic efficiency can reach 54%. The most significant aspect of this electrode is reusability: that is, upon reversal of the electrode voltage, the uranium deposited in the foam can be ejected into a solution 40× more concentrated than the original wastewater. We have demonstrated no uranium extraction capacity fading in the solution during the first seven cycles. Moreover, we have succeeded in reducing uranium concentration in spiked seawater from 3 ppm to 19.9 ppb, which is lower than the US EPA uranium limits for drinking water (30 ppb). We attribute the good uranium electrochemical extraction performance of the 3D-FrGOF to the following reasons: good HER catalysts that can cause effective local pH increase during HER; suitable surface condition that can coordinate with uranium species; large surface area and good mechanical robustness.

2. Results and Discussion

3D-FrGOF was synthesized by a hydrothermal process, during which the rich functional groups on graphene oxide will react with ethylenediamine (EDA), polysulfides, polythiobisamines, and free polysulfides radical species to obtain the sulfur and amine-modified graphene foam.^[8] Sulfur plays a vital role in sustaining the physical stability and flexibility of the foam. The electrolytic uranium extraction was achieved in a three-electrode system, and the details of the setup are shown in Figure S1 in the Supporting Information. The functionalized 3D-FrGOF is the working electrode, and the functional groups on the graphene surface can form chelation binding with the uranium ions in the solution. Figure 1a,b show the process of the electrolytic deposition. When a negative potential of -0.9 V vs SCE was applied to the working electrode, cations moved to the working electrode, and uranium cations would be complexed by the functional groups. Under such potential, the local pH value of the electrode will increase significantly, which is mainly due to HER of water.

Oxygen reduction reaction (ORR) of the dissolved oxygen in the solution also contributes to the local pH increase. Because the amount of dissolved oxygen is limited, our analysis points to HER as the main driver of pH increase here. The HER and ORR reactions are shown in Figure S1, Supporting Information, and both reactions generate OH⁻ anion. Under the much-increased local pH with an applied electric field, uranium cations can deposit and grow on the electrode. On the other hand, the global pH of the solution does not change much, because the counter electrode undergoes oxygen evolution reaction that generates excess H⁺ (and locally low pH) that balances the OH⁻ diffusing out from the working electrode, in most of the water body.

Figure 1c–e shows the photograph and scanning electron microscopy (SEM) images of the 3D-FrGOF. The foam is of round shape, and the thickness is ≈1 mm. The surface of the foam is flat, and the inner structure is porous. This structure enabled high reaction surface area, and at the same time, the structure can survive the mechanical impact of gas generation. As shown in Figure S2, Supporting Information, the foam is flexible, and after pressing with a weight of 5000 times of its own weight. It can recover quickly to its original size, which indicates the excellent mechanical property for long-term use. The pore sizes are uniform with the mean value ≈10 μm. The BET surface area of the foam is 115 m² g⁻¹ as determined by N₂ adsorption-desorption isotherm.

Un-doped reduced graphene oxide foam without elemental doping (3D-rGOF) was synthesized for comparison. Fourier-transform infrared spectra (FTIR) of 3D-FrGOF and 3D-rGOF are shown in Figure 1f. Both samples show the peaks at 3440 cm⁻¹ for the stretching vibration of O–H, indicating that there remained a lot of –COOH and –OH functional groups on reduced graphene oxide after the hydrothermal process.^[9] However, the 3440 cm⁻¹ peak of 3D-FrGOF is broader, that is caused by the overlap of vibration of O–H and N–H. The two peaks at 2927 and 2855 cm⁻¹ are C–H stretching vibrations.^[10] Several new peaks are shown in the 3D-FrGOF sample. The peak at 1624 cm⁻¹, corresponding to the in-plane vibration of C=C, shift to 1570 cm⁻¹ due to the overlap of the vibrations of C=C and C=N and bending of N–H, which indicate the binding of the

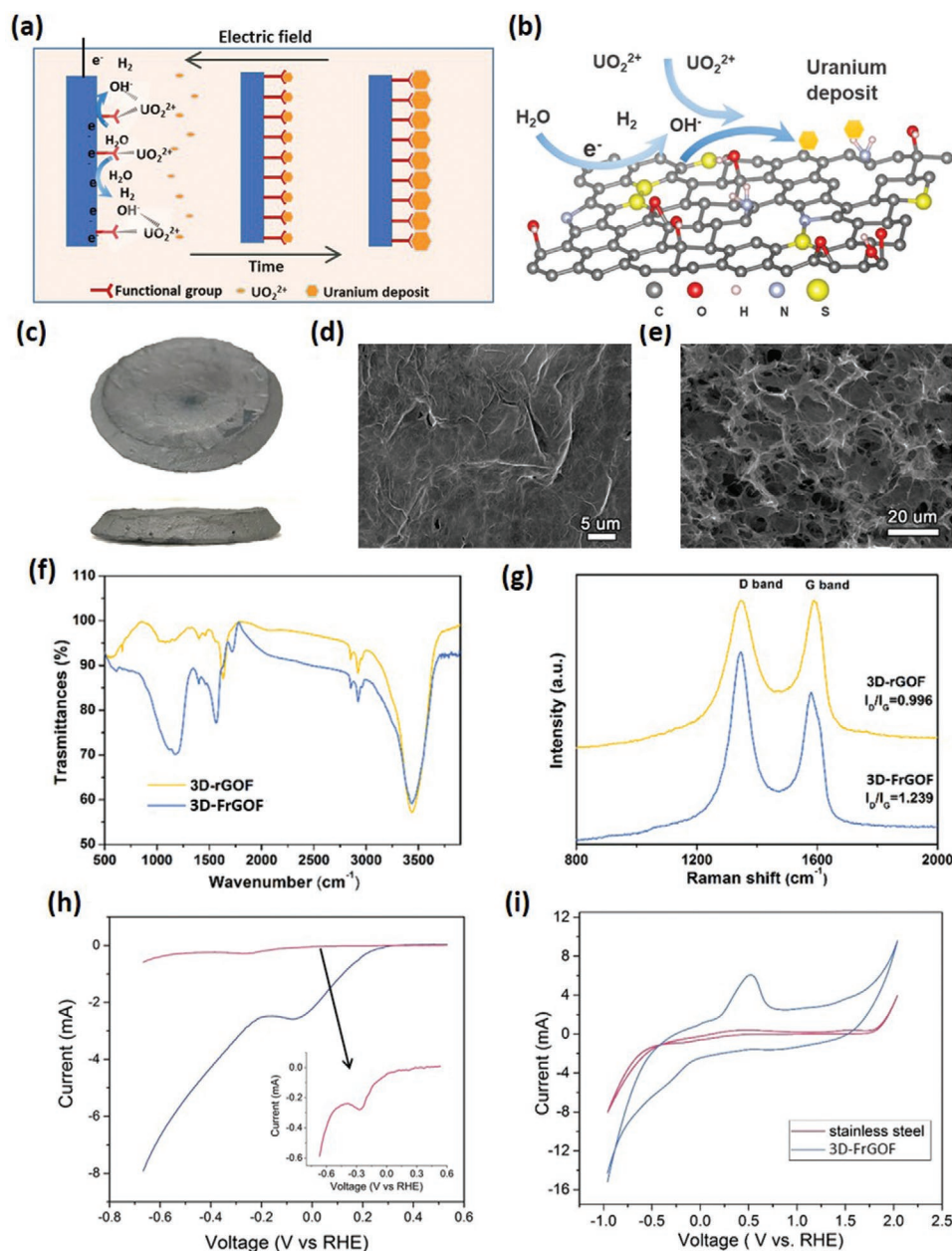


Figure 1. a,b) Schematics of the electrolytic deposition process of uranium. c–e) Photograph and SEM images of the surface and inner part of 3D-FrGOF. f,g) Raman and FTIR spectra of 3D-FrGOF and 3D-rGOF. h) Polarization curves of 3D-FrGOF electrode and stainless steel holder in blank solution with a scan rate of 5 mV s⁻¹. i) CV curves of the 3D-FrGOF electrode and stainless-steel holder in 100 mg L⁻¹ uranium solution.

amino-functional group with the graphene oxide.^[11] The significant broad peaks at 1176 and 1124 cm⁻¹ are the vibration of C–N and C–S, this proves the sulfur doping in the graphene.^[12] The peak at 1720 cm⁻¹ is the C=O stretching vibration of COOH groups. In the blank 3D-rGOF sample, this peak shifted and overlapped with the C=C vibration in graphene oxide.^[9,13]

X-ray photoelectron spectroscopy (XPS) of the 3D-FrGOF further confirms the FTIR results. Compared to the blank 3D-rGOF, 3D-FrGOF shows the signal of nitrogen and sulfur in the survey spectrum. High-resolution spectra of N 1s and S 2p are shown in Figure S3, Supporting Information. There are three types of nitrogen in 3D-FrGOF, and amino N (65%) is the

dominant type. The other two are pyridinic- and graphitic-type N, which are the main sources of C–N in 3D-FrGOF.^[14] S 2p mainly shows the peaks of C–S (66%) and high oxidation sulfate or sulfonate in the composite. The amino-, pyridinic-N, and C–S can provide lone-pair electrons, which can coordinate with metal cations. In addition, sulfate/sulfonate can adsorb uranium cations during the electrolytic deposition process.

Raman spectra of 3D-rGOF and 3D-FrGOF displayed in Figure 1g show two prominent peaks at ≈1589 and 1347 cm⁻¹, this corresponds to the G band and D band associated with the vibration of sp² and sp³ carbon atoms of defects and disorder in the graphene materials. The intensity ratio of D to G bands,

$R \equiv I_D/I_C$, can be used to evaluate the extent of structural defects. The R values of 3D-rGOF and 3D-FrGOF are 0.996 and 1.239, respectively. The higher R values of the 3D-FrGOF can attribute to the elemental doping and functional group modification on the surface of the reduced graphene oxide.^[15]

The electrochemical property of 3D-FrGOF was first studied in a blank solution without uranium. The pH of the solution is 5.2, which is consistent with the uranium extraction, as we will discuss later. For analysis, the electrochemical performance of a 316 stainless steel electrode holder is also studied. Polarization curves were obtained by linear sweep voltammetry (LSV) at a scan rate of 5 mV s⁻¹ at room temperature. A saturated calomel electrode (SCE) was used as the reference electrode for all the electrochemical tests, and the potential was calibrated to a reversible hydrogen electrode (RHE). 3D-FrGOF shows enhanced reduction current while stainless steel displays a much lower current, a magnified view inserted in Figure 1h. Both HER and ORR should contribute to the reduction current of the samples. The reduction peaks at -0.06 and -0.2 V vs RHE (-0.6 and -0.74 V vs SCE) for 3D-FrGOF and 316 stainless steel, respectively, should be attributed to the reduction of O₂. For HER, 3D-FrGOF displayed an onset potential of -0.18 V vs RHE (-0.72 V vs SCE), while stainless steel showed an onset potential at -0.41 V vs RHE (-0.95 V vs SCE). Cyclic voltammetry (CV) curves of the 3D-FrGOF electrode and the stainless steel holder in 100 mg L⁻¹ uranium solutions (100 ppm) are shown in Figure 1i. HER and ORR happen at the working electrodes, which was similar to the LSV results. 3D-FrGOF electrode showed a much larger current than the holder. A broad ORR peak at ≈-0.18 V vs RHE (-0.72 V vs SCE) can be observed for 3D-FrGOF, and perceptible HER current can be seen during the cathodic scan. CV curves at different conditions without uranium in the electrolyte are shown in Figure S4, Supporting Information. Before applying a current, we flowed N₂ and O₂ gas for 1 h into the electrolyte to analyze the effect of oxygen reduction. During the cathodic scan, oxygen reduction happened first at ≈0.24 V vs RHE (-0.3 V vs SCE) with enhanced current, which certified the existence of ORR current in the air (Figure 1i). The de-oxygenated electrolyte saturated by nitrogen gas showed no oxygen reduction because of no soluble oxygen in the solution. The electrolyte saturated by oxygen gas showed a high reduction current, which is due to the contribution of the enhanced ORR current. The oxidation peaks at 0.55 V vs RHE were shown in both uranium contained solution and non-uranium solution, indicating these peaks should be related to the oxidation of the graphene materials or the holder.

2.1. Extraction Performances

The extraction performance of the 3D-FrGOF electrode was studied as a function of pH, applied voltage, time, and initial uranium concentration. Cycling performance was carried out to investigate the reusability of the 3D-FrGOF electrode. The initial concentration of uranium is presented by C_0 (in unit of mg L⁻¹, with 1 mg L⁻¹ ≈ 1 weight ppm). After extraction, the residual uranium concentration (C_r) was determined by inductively coupled plasma (ICP). The uranium specific extraction capacity q of the 3D-FrGOF electrode was calculated by the following equation:

$$q \equiv \frac{(C_0 - C_r)V}{m_0} \quad (1)$$

where m_0 is the original mass of the working material, and V is the volume of the liquid solution.

2.1.1. Effect of pH

pH is an essential factor for electrolytic uranium extraction due to the variable uranium complexes at different pH.^[16] The pH influence on the U(VI) deposition was investigated in detail over a pH range from 2 to 8 at $C_0 = 100 \text{ mg L}^{-1}$ for 2 h. The voltage applied to the electrolytic cell is -0.9 V. Figure 2a shows the uranium extraction specific capacity against pH of the 3D-FrGOF electrode. When the pH is as low as 2, the extraction capacity is only 50 mg g⁻¹. Under a low pH, the proton concentration is high, and the local pH increase will be much less than the higher pH. At pH 4, the extraction capacity increases significantly to 720 mg g⁻¹, and with further increase of the pH to 5.2, we get the highest capacity of 1173 mg g⁻¹, which is 95% removal of uranium in the system. When pH increased to 6, 7, and 8, the specific capacity keeps decreasing. This is caused by the change of uranium species from cations to anions. At a lower pH under 6, The dominant species are expected to be monomers UO₂²⁺ and UO₂OH⁺, the dimer (UO₂)₂(OH)₂²⁺, and the trimer (UO₂)₃(OH)₅⁺. At pH above 7, the monomer UO₂(OH)₃⁻ and the trimer (UO₂)₃(OH)₇⁻ become the most dominant species.^[6,17] The change of uranium species from cations to anions changed the double-layer construction, which leads to decreased interaction between uranium species and the functional groups on 3D-FrGOF. Due to the highest electrolytic extraction capacity was obtained at pH = 5.2, the initial pH value of the system was set as 5.2 for further experiments.

2.1.2. Effect of the Applied Voltage

Applied voltage plays a critical role in our electrolytic deposition. Experiments were carried out at various negative potentials in the range of -0.3 to -1.5 V vs SCE at pH = 5.2 and $C_0 = 50 \text{ mg L}^{-1}$ uranium solution. The results plotted in Figure 2b indicated that increasing the applied voltage to more negative values from -0.3 to -0.9 V gave a progressive improvement in electro-extraction efficiency of U(VI), from 47 to 98%, respectively. According to the Pourbaix diagram of water (Figure S5, Supporting Information), at pH = 5.2, the potential that hydrogen begins to generate is -0.3 V vs SHE and -0.54 V vs SCE. From CV and the constant voltage curve (Figure S6, Supporting Information), we can see that the current at -0.3 V is much lower than -0.9 V, indicating that the water reduction reaction at the working electrode is much less than at -0.9 V. When there is not much water reduction reaction, the pH increase around the electrode is smaller, and uranium deposition is more difficult. At -0.3 V, the extraction capacity is 350 mg g⁻¹. This extraction capacity is much higher than the absolute chemical adsorption capacity of 3D-FrGOF toward uranium. The chemical adsorption capacity was obtained by

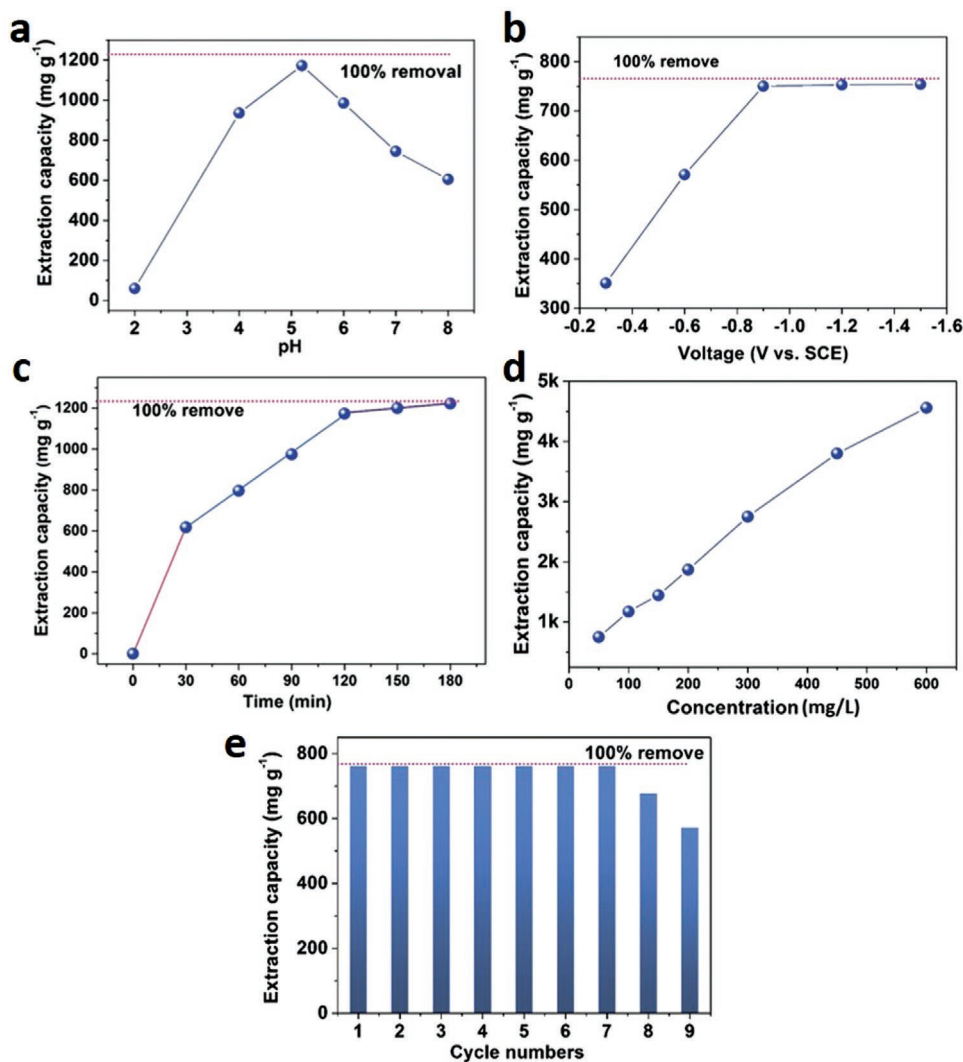


Figure 2. Extraction performance at different conditions: a) Effect of pH at 100 mg L⁻¹ uranium. b) Effect of applied voltage at 50 mg L⁻¹ uranium. c) Effect of time at 100 mg L⁻¹. d) Effect of concentration. e) Cycling performance of the uranium extraction at 50 mg L⁻¹.

a solid-phase extraction experiment, which shows a uranium extraction capacity of 223 mg g⁻¹. Details of the solid phase extraction are shown in the supporting materials. The much increased extraction capacity at -0.3 V is caused by the uranium electrolytic deposition process, which is induced by the increase of local pH during the ORR. When decreasing the voltage to -0.9 V, the specific extraction capacity increased significantly to 750 mg g⁻¹, this is caused by the dramatic increase of local pH generated by HER on the working electrode. Further lowering of the applied potential to a more negative potential (-1.2, -1.5 V vs SCE) can also maintain more than 99% uranium removal, but less energy-efficient. Therefore, the potential was set to -0.9 V vs SCE for the further studies.

2.1.3. Effect of Time

Different extraction time was used to optimize the extraction efficiency, and the results in 100 mg L⁻¹ uranium solution are shown in Figure 2c. pH and voltage were adjusted to be 5.2 and -0.9 V,

respectively, as optimized by the experiments above. After 30 min of extraction, 52.6% uranium was removed from the solution. 67.9% and 83% of uranium were removed at 1 and 1.5 h, respectively. After 2 h, 95% uranium was removed, and 99% uranium was removed after 3 h. Longer time can achieve higher uranium extraction, but the deposition kinetics becomes slower with the increase of time. The deposition rate at the first 30 min is the fastest, which is 20.58 mg (g·min)⁻¹. From 30 min to 2 h, the deposition process became slower, with a rate of 6.98 mg (g·min)⁻¹. After 2 h, the deposition speed was only 0.82 mg (g·min)⁻¹. The first 2 h is much more effective than the last 1 h, since only 4% of the uranium removal occurred in the last 1 h. Unless otherwise specified, we used 2 h for the presentation.

2.1.4. Effect of Concentration

As shown in Figure 2d, the extraction capacity at different uranium concentrations (C₀): 50, 100, 150, 200, 300, 450, and 600 mg L⁻¹ in the electrochemical cell for 2 h were studied.

The specific capacity increases with increasing C_0 . The highest extraction capacity is 4560 mg g^{-1} at 600 mg L^{-1} , and the corresponding Coulombic efficiency is 54%. Details of the calculation are shown in the experiment part. The highest removal percentage for 2 h is 98% at 50 mg L^{-1} . The residual uranium concentration is $\approx 1 \text{ mg L}^{-1}$. We also did the 6 h extraction experiment, and 99.5% uranium was removed.

The electrolytic extraction capacity of the blank 3D-rGOF electrode in 100 mg L^{-1} uranium solution is 365 mg g^{-1} , which is much lower than the 3D-FrGOF with a capacity of 1173 mg g^{-1} , indicating that the functional groups play a critical role in the electrolytic deposition. The chemical adsorption capacity of the 3D-FrGOF material obtained by the solid-phase extraction method at 100 mg L^{-1} was 360 mg g^{-1} . The much higher extraction capacity of the electrolytic deposition method compared to the chemical adsorption method is coming from the continuous electrochemical reaction that increases the local pH near the electrode. The absolute adsorption capacity of 3D-FrGOF is already much higher than many other adsorption materials in the literature,^[18] which demonstrates the functional groups modification on 3D-FrGOF is effective. These functional groups act as ligands that can coordinate with uranium cations. Without the functional groups, the blank graphene oxide foam shows a low adsorption capacity of 75 mg g^{-1} . We assume that uranium cations will first coordinate with the functional groups and be fixed on the graphene matrix, and then deposit under a certain potential. Besides, the functionalized graphene material can decrease the overpotential of the ORR and HER compared to blank reduced graphene oxide foam, so the increase of local pH under the same potential can be more significant. Thus, the nucleation barrier for the deposition product is decreased, and much higher extraction capacities can be achieved.

2.1.5. Cycling Performance

The uranium deposit on the electrode can be released by a dissolution process, which is done under an applied potential of 2.0 V vs SCE for 2 h. At 2.0 V, water will be oxidized to oxygen gas on the working electrode and release protons. This can decrease the local pH of the electrode and promote the dissolution of uranium-bearing solid compound. Cycling performance is studied to check the reusability of the 3D-FrGOF electrode. After electrolytic deposition in 50 mg L^{-1} uranium solution, the uranyl species were released by mechanically moving the electrode into a second, highly concentrated bath (2000 mg L^{-1} uranium solution), and reversing the polarity of the applied voltage. This regenerated electrode was placed back in another 50 mg L^{-1} solution for the next extraction. Several cycles of deposition and dissolution were done.

Figure 2e shows the extraction capacity of the 3D-FrGOF electrode for nine cycles. The initial extraction capacity is 761 mg g^{-1} and remains stable in the first seven cycles. The extraction capacity decreases to 85% and 75% of the initial capacity at the 8th and 9th cycle. During cycling, there is no visible damage of the electrode, i.e. exfoliation or formation of cracks, indicating that the structure of the 3D-FrGOF electrode is robust under both oxidation and reduction environments. The decay of the extraction capacity may have been caused by the loss of

functional groups on the electrode. Also, we observed some cracks at the place where the holder and the electrode were in contact, which is caused by the mechanical movement of the holder when we handle the electrode. The structure of the holder should be better designed to maintain the electrode integrity.

Table S1, Supporting Information, listed the comparison of our work with some previous reports. Electrochemical extraction method is much more efficient than the chemical adsorption method. Compared to other electrochemical methods such as electro-coagulation, capacitive deionization, etc., our electrode is much more stable and efficient. The in situ uranium extraction is clean with high Coulombic efficiency, and the extracted uranium can be easily discharged to be enriched.

2.2. Characteristics of the Uranium Deposit and Mechanism Discussion

After the electrolytic deposition in 100 mg L^{-1} solution for 2 h, the color of the uranium solution clearly changed. Figure 3a1 shows the photograph of the solution before and after the electrolytic deposition, the colorless solution after extraction indicates that most of the uranium species are removed by the 3D-FrGOF electrode. For the solution extracted by blank 3D-rGO foam, the color is still pale yellow, indicating the uranium extraction is not as thorough. After electrolytic deposition, the surface of the 3D-FrGOF electrode is covered by a yellow deposit, which can be observed clearly by the photographs of the electrode after drying in Figure 3a2.

SEM images of the 3D-FrGOF electrode after uranium deposition are shown in Figure 3b,d. The surface-covering uranium-containing solid phases are grown densely packed. Figure 3c shows the SEM image of the yellow powder that was peeled off from the 3D-FrGOF electrode and was sonicated in ethanol. The morphology of the flake is a hexagon-like shape with a size ranging from 500 nm to 1 μm . The array-like deposits (Figure 3d) consist of the lateral face of the hexagon-like flakes. This indicated that the lateral face of the hexagon-like flakes is easier to bind with the 3D-FrGOF surface and the deposits grow up along the perpendicular direction when the uranium species deposit on the electrode surface. The energy spectrum (Figure S7, Supporting Information) and elemental mapping of uranium and oxygen are shown in Figure 3e,f. The surface covering species consists mainly of uranium, oxygen, and carbon. There is a small amount of sodium, nitrogen, and sulfur on the electrode, caused by the sodium cations in the solution and the ethane diamine and sulfur modified rGO.

Figure S8, Supporting Information, displays the XPS survey of the 3D-FrGOF electrode before and after the uranium deposition. It is obvious that the electrode surface consists mainly of uranium and oxygen. The very weak sodium signal indicates that there is almost no sodium extraction during this electrolytic deposition process. The carbon signal is also weak due to the full coverage of uranium species on the electrode surface. Figure 4a shows the high-resolution XPS spectra of the U 4f orbital. The binding energy separation between primary and associated satellite peak (ΔE_{s-p}) is a function of U 4f binding energy for different oxidation states. Here, U $4f_{5/2}$ and $4f_{7/2}$ are located at 392.5 and 381.6 eV. The shake-up satellite

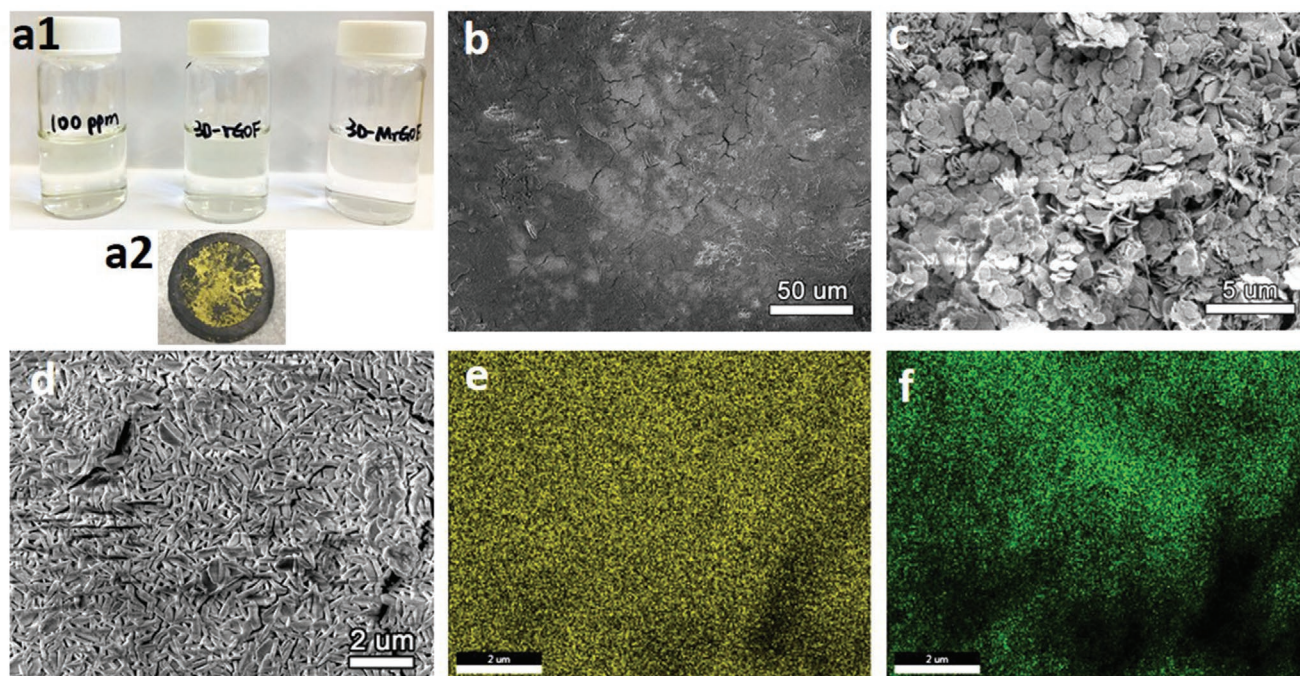


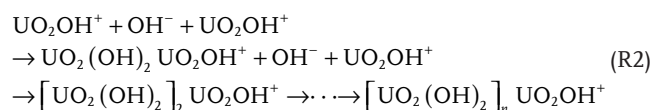
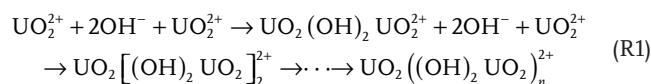
Figure 3. a) Photograph of the uranium-contaminated solution before and after extraction with blank 3D-rGOF and 3D-FrGOF and the photograph of 3D-FrGOF after uranium extraction. b) SEM images of the 3D-FrGOF electrode after uranium deposition. c) SEM of the deposit after sonication, d) SEM of the 3D-FrGOF surface, and e, f) the corresponding elemental EDX mapping of uranium (e) and oxygen (f).

peaks appear at a distance of 3.5 eV from these main peaks. Another U $4f_{5/2}$ satellite peak at 9.5 eV away from the primary peaks is also observed. The FWHM of U $4f_{5/2}$ and $4f_{7/2}$ peaks are ≈ 1.6 eV.^[19] Figure 4b XANES data also proves the hexavalent state of uranium. The oxidation state of the deposited uranium compound is the same as the standard $\text{UO}_2(\text{NO}_3)_2$ solution. No U(IV) can be observed in the deposit, indicating there is no uranium reduction in the electrolytic deposition process. This is consistent with the CV result in Figure 1i, where we did not observe the uranium reduction peak. However, from the Pourbaix diagram of uranium in Figure S9, Supporting Information, uranium should be reduced under -0.9 V vs SCE. Possible reasons of why there was no uranium reduction are: 1. The overpotential required to reduce uranium from U(VI) to U(IV) could be high. This leads to the need for more negative potential than that of the hydrogen reduction reaction. Therefore, under the -0.9 V potential that we applied here, HER reaction dominates the reaction, evidenced by the absence of a uranium reduction peak in the CV curve; 2. Even if the reduction can occur after the solid deposition on the electrode surface as a result of local pH increase, it will be limited at the electrode– $\text{U}(\text{OH})_x$ interface, due to the electronically insulating nature of the deposit. The electron cannot propagate further to reduce the $\text{U}(\text{OH})_x$ particle. The Pourbaix diagram of uranium in Figure S9, Supporting Information, shows that the deposition should be $\text{UO}_2(\text{OH})_2$ polymorphs.

Raman and FTIR spectra of the 3D-FrGOF electrode after uranium electrolytic deposition are shown in Figure 4c,d. The new strong peak at 874 cm^{-1} is the stretching vibration of U–O.^[20,21] The peak at 746 cm^{-1} is the stretching vibration of O–U–O–U.^[22] Peaks observed at lower wavenumbers

$\approx 300\text{ cm}^{-1}$ can be assigned to the bending vibrations of $(\text{UO}_2)^{2+}$ or stretching vibration of U–O.^[21] From the FTIR spectrum, the two intensive adsorption bands at 3438 and 1612 cm^{-1} correspond to O–H stretching and bending, respectively. The very broad peak at 3438 cm^{-1} may be due to the overlap of OH in uranium oxide hydroxide. The new peak at 983 cm^{-1} is the vibration of U–N, which proves the coordination of $-\text{NH}_2$ with uranium species during the deposition process.^[20,23,24] The new peak of 1350 cm^{-1} is the vibration of N–O, which may come from the uranium nitrate in the electrolyte. The peak at 1176 cm^{-1} of C–N vibration in the 3D-FrGOF can hardly be observed after the uranium deposition due to coordination of uranium with the amide groups.

The deposition of uranium oxide hydroxide during the electrolytic process is in 2D sheet-like structure, which is consistent with the reported structure of uranium oxide hydroxide.^[23] The formation of this sheet is probably associated with the double OH bridges in the compound.^[25,26] UO_2^{2+} ion undergoes hydrolysis and polymerization when the pH is raised. Deposition occurs when polymerization has proceeded to a point where the species is no longer soluble.^[27] At pH = 5.2, the uranium in the solution is mainly UO_2^{2+} and UO_2OH^+ . The electrolytic deposition can be described as follows:



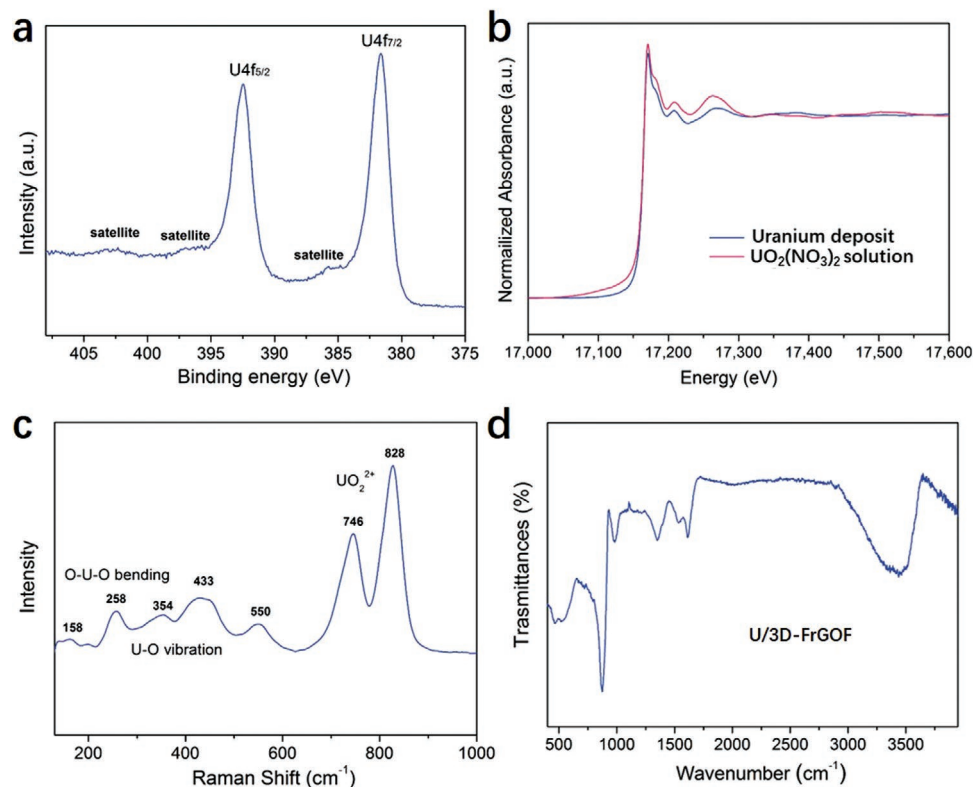


Figure 4. a) High-resolution XPS spectra of the U4f in the 3D-FrGOF after uranium deposition. b) XANES spectra of the uranium deposit and standard UO₂(NO₃)₂. c) Raman and d) FTIR spectra of the 3D-FrGOF electrode after uranium deposition.

Both UO₂((OH)₂UO₂)_n²⁺ and [UO₂(OH)₂]_nUO₂OH⁺ after deposition can be simplified as UO₂(OH)₂, which is consistent with our previous analysis. We note that Reaction (R1) and (R2) are pure chemical reactions, not electrochemical redox reactions that involve long-range transfer of electron from external metallic circuit. Thus, the Coulombic efficiency in this paper is defined based on the number of uranium(VI) harvested on the 3D-FrGOF electrode per electron transferred across the outer circuit, not the number of uranium(VI) undergoing redox. Most of those electrons drive HER/ORR and local pH change, which shifts the location on the Pourbaix diagram, and the negative voltage also attracts uranium(VI) to come to the 3D-FrGOF and facilitates nucleation and growth, but those electrons did not induce uranium redox as the uranium ions stay predominantly 6+ throughout the process. This is why we call our process “electrolytic deposition”, and not electrodeposition which typically involve reduction of the metallic species deposited.

The crystal structure of the deposit was checked using an X-ray wavelength of 0.01173 nm to obtain more information on the structure. **Figure 5a** shows the synchrotron XRD curve after extraction of the background and transferred into the typically used wavelength of 0.154 nm. However, no existing XRD pattern from the database can be assigned to the obtained deposit. In order to explore the atomic structure of our material, we performed first-principles density functional theory (DFT) calculations, under hexagonal lattice symmetry based on transmission electron microscopy (TEM) results. As shown in **Figure 5b** our optimized structure shows a quasi-2D UO₂(OH)₂

layer stacked pattern. In each layer, the U atoms form a trigonal lattice. Each U–U pair is bonded by two OH at the bridge site, the other two O atoms are vertically bonded with each U atom (top and bottom sites). The optimized stacking pattern is when these top and bottom O form hydrogen bonds with the H in the nearest neighbor layers, which makes each unit cell is composed of three UO₂(OH)₂ layers. The space group of this structure is *R*-3*m* with lattice constants of *a* = *b* = 4.05 Å and *c* = 17.19 Å. We also calculate its formation energy to be –2.60 eV/atom, which is comparable with the *Pbca*-U(HO₂)₂ phase (–2.62 eV/atom). The calculated XRD spectrum agrees well with the experiment, confirming this atomic structure. The broad peak at 26° is the overlap of the second and third strongest peaks. The .cif document of the crystal structure is provided in the supporting materials.

TEM images of the particles are shown in **Figure 5c**. The particles show the morphology of hexagonal-shaped thin disks. The selected area electron diffraction (SAED) pattern shown in **Figure 5d** is very similar to a sixfold symmetry crystal structure. The SAED pattern is also consistent with the proposed crystal structure, which is labeled in **Figure 5d**. The labeled crystal planes correspond to the two very close XRD peaks, which overlap to become the second broad peak of XRD in **Figure 5a**. A similar crystal structure had been proposed in the early 1950s.^[25] However, only one layer of the atom stack has been assumed, and no crystal data were provided. With the help of synchrotron diffraction and DFT calculation, we obtained the structure information, and the experimental TEM diffraction

data agrees well with the calculated structure. The simulated pair distribution function of the composite from the reconstructed crystal structure matches well with the experimental one, which was shown in Figure S10, Supporting Information.

we achieve a capacity of 4560 mg g^{-1} without saturation. Moreover, 3D-FrGOF electrode succeeded in removing uranium from spiked seawater to lower than the EPA uranium limit for drinking water (30 ppb).

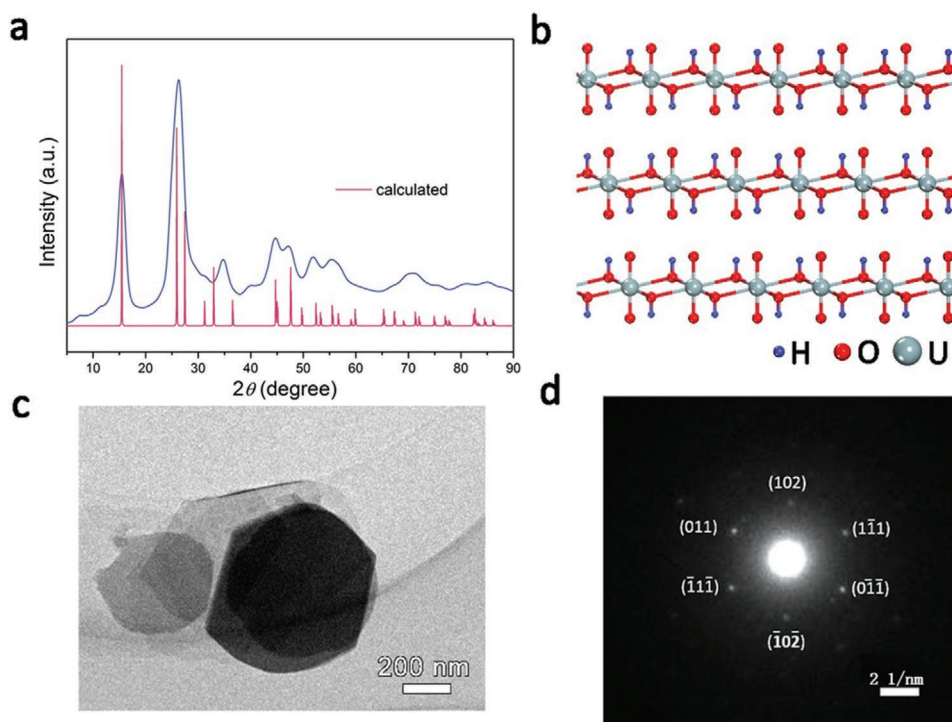


Figure 5. a) XRD of the 3D-FrGOF electrode after uranium extraction and the calculated XRD. b) Calculated atomic structure of the uranium deposit. c) TEM image of the uranium deposit. d) SAED pattern of the uranium deposit with the identification of the crystal planes.

Encouraged by the outstanding electrolytic deposition capacity and impressive electrolytic deposition kinetics in pure U(VI) solution, we further studied the extraction performance of the removal of uranium in spiked seawater with a concentration of 3 mg L^{-1} , which is 100 times higher than the EPA limit in drinking water (30 ppb). The 3D-FrGOF electrode has succeeded in decreasing uranium concentration in spiked seawater from 3 mg L^{-1} to less than 19.9 ppb within 14 h (note this treatment time is longer than the default 2 h), which met the US EPA requirement for drinking water. The high concentration of seawater salt (2.4 wt% NaCl, 1.1 wt% MgSO_4 , 0.4 wt% Na_2SO_4 , etc.) clearly did not influence too much our uranium electrolytic deposition process.

3. Conclusion

Most of the uranium extraction research focused on chemical and physical adsorption. Electrochemical extraction had also been studied in several articles, and most of them deposited on Al and Ni electrode with a much negative potential.^[28] Compared to the reported electrochemical extraction methods, our Coulombic efficiency (up to 54%) and extraction capacity are very high. By using electrocatalysts of the functional graphene foam, which can lead to effective local pH increase,

3D-FrGOF electrode doped with sulfur and nitrogen has been synthesized using a hydrothermal method. The functional groups play an essential role in the electrolytic deposition, and the extraction capacity is much higher when compared to the blank rGOF. Moreover, uranium can be efficiently ejected out from the used electrode into a second bath of much higher uranium concentration of 2000 ppm, 40 times higher than the industrial sewage concentration (50 ppm), for 7 cycles. The loss in extraction capacity and efficiency does not exceed 15% after nine electrosorption/desorption cycles. The structure of the solid deposit was calculated by DFT calculation, which shows a quasi-2D $\text{UO}_2(\text{OH})_2$ layered crystal structure.

The results above suggest a cheap and sustainable 3D-FrGOF electrode for the in situ uranium removal from contaminated water, nuclear effluents, nuclear waste cleanup, etc. It opens new opportunities in using functional graphene foam electrode as a novel platform for nuclear waste treatment and environmental remediation.

4. Experimental Section

Materials Synthesis: Graphene oxide was first synthesized using a modified Hummer method and the details are shown in our previous article.^[29] The 3D-FrGOF was made by a hydrothermal process with the assistance of sulfur and EDA. Typically, 16 mL 3 mg mL^{-1} graphene

oxide was mixed with 200 mg sulfur, which was dissolved into 2 mL EDA, under vigorous stirring for 10 min. Then the mixture solution was put into a self-designed pie-shaped Teflon-lined autoclave for the hydrothermal reaction at 180 °C for 12 h. Then, self-assembled 3D-FrGOF was washed with DI water several times and freeze-dried. The blank 3D-rGOF was made in the same way without adding sulfur and EDA. Uranium standard ICP solution was bought from Ricca Chemical and artificial seawater was bought from Merck.

Materials Characterization: The morphology was observed by field-emission SEM (FESEM) (Zeiss Merlin high-resolution scanning electron microscope) and TEM (JEOL-2010F, 200 kV). The local chemical analysis was performed by EDX (energy dispersive X-ray analysis) in the SEM. FTIR measurement was carried out on Thermo Fisher FTIR6700. Raman spectroscopy was measured from 100 to 3000 cm^{-1} on a Renishaw Invia Reflex Micro Raman with an excitation wavelength of 532 nm. XPS measurement was carried out on a PHI Versaprobe II XPS (aka ESCA) imaging photoelectron spectrometer using a monochromatized Al $K\alpha$ radiation. The energy calibrations were made against the C 1s peak. Inductively coupled plasma–optical emission spectroscopy (ICP-OES, Agilent, 5100 DVD) and inductively coupled plasma mass spectrometry (ICP-MS, Agilent 7900) were used to analyze the uranium concentration. Synchrotron XRD with a wavelength of 0.01173 nm was performed at Argonne National Lab. X-ray adsorption spectroscopy spectra of U L edge were collected under a fluorescence mode at Beamline 07A1 at the National Synchrotron Radiation Center in Taiwan, which was operated with an electron energy of 1.5 GeV. Monochromatic X-ray was produced with a Si(111) double-crystal monochromator.

Uranium Extraction Experiment: The electrolytic deposition was done in a three-electrode system. The working electrode holder was made of 316 stainless steel, the counter electrode was Pt wire, and the reference electrode was a SCE. Constant voltage was applied to the working electrode for the extraction by a Gamry workstation. The tested uranium solution was diluted to a certain concentration from the ICP standard solution of 1000 mg L^{-1} (Inorganic Ventures, CGU1) and the 2000 mg L^{-1} uranium solution was diluted from 10000 mg L^{-1} (VWR Chemicals BDH, Aristar). Artificial seawater (Ricca Chemical Company, CAT 8363-1, with 2.39 wt% sodium chloride, 1.08 wt% $\text{MgCl}_2 \cdot 6\text{H}_2\text{O}$, 0.4 wt% Na_2SO_4 , 0.15 wt% $\text{CaCl}_2 \cdot 2\text{H}_2\text{O}$, 0.07 wt% KCl, 0.02 wt% NaHCO_3 , etc.). The pH was tested by a Thermo Scientific pH meter and was adjusted by sodium hydroxide and nitric acid. After extraction, the solution was collected for ICP-OES or ICP-MS test. The total charge (in Coulomb) was calculated by the integration of current–time curve. The number of electrons (in mol) was calculated via dividing the total charge by the Faraday constant (96485 C mol^{-1}). 1 mole electron should ideally correspond to 1 mole OH^- or 0.5 mole uranium. The uranium mole amount (#(uranium deposited)) is calculated by the (extraction mass)/(304 g mol^{-1} based on $\text{UO}_2(\text{OH})_2$). Coulombic efficiency \equiv #(uranium deposited) / 0.5# electron.

DFT Calculations: DFT calculations are based on Perdew–Burke–Ernzerhof treatment for the exchange–correlation term, as implemented in the Vienna ab initio simulation package.^[30] The core and valence electrons were treated using projector-augmented wave method^[31] and a plane wave basis set with a cutoff energy of 400 eV, respectively. The first Brillouin zone was represented by a Γ -centered Monkhorst–Pack k -mesh^[32] with grid dense of $2\pi \times 0.02 \text{ \AA}^{-1}$. The convergence criteria of total energy and force component were set to 1×10^{-4} eV and 0.01 eV \AA^{-1} , respectively. Van der Waals interactions in Grimme's D3 correction method have been included.^[33]

Supporting Information

Supporting Information is available from the Wiley Online Library or from the author.

Acknowledgements

C.W. and A.S.H. contributed equally to this work. J.L. would like to acknowledge support by DTRA (Award No. HDTRA1-20-2-0002)

Interaction of Ionizing Radiation with Matter (IIRM) University Research Alliance (URA).

Conflict of Interest

The authors declare no conflict of interest.

Data Availability Statement

The data that support the findings of this study are available from the corresponding author upon reasonable request.

Keywords

electrolytic deposition, extraction capacity, graphene foam, local pH, nuclear energy, reusability, uranium extraction

Received: April 7, 2021

Revised: May 12, 2021

Published online: August 4, 2021

- [1] a) M. M. Abu-Khader, *Prog. Nucl. Energy* **2009**, *51*, 225; b) C. Degueldre, J. Bertsch, G. Kuri, M. Martin, *Energy Environ. Sci.* **2011**, *4*, 1651.
- [2] a) S. Nagasaki, in *Reflections on the Fukushima Daiichi Nuclear Accident*, (Eds: J. Ahn, C. Carson, M. Jensen, K. Juraku, S. Nagasaki, S. Tanaka), Springer International Publishing, New York **2015**, p. 297; Uranium Mining Overview (updated December 2020), World Nuclear Association; <https://www.world-nuclear.org/information-library/nuclear-fuel-cycle/mining-of-uranium/uranium-mining-overview.aspx> (accessed: July 2021).
- [3] A. Chen, C. Shang, J. Shao, J. Zhang, H. Huang, *Sci. Total Environ.* **2017**, *575*, 1291.
- [4] a) K. Vaaramaa, S. Pulli, J. Lehto, *Radiochim. Acta* **2000**, *88*, 845; b) S. Y. Lee, E. A. Bondietti, *J. Am. Water Works Assoc.* **1983**, *75*, 536; c) I. A. Katsoyiannis, H. W. Althoff, H. Bartel, M. Jekel, *Water Res.* **2006**, *40*, 3646; d) C. S. Barton, D. I. Stewart, K. Morris, D. E. Bryant, *J. Hazard. Mater.* **2004**, *116*, 191.
- [5] a) T. J. Sorg, *J. Am. Water Works Assoc.* **1988**, *80*, 105; b) J. Shen, A. Schäfer, *Chemosphere* **2014**, *117*, 679.
- [6] I. A. Katsoyiannis, A. I. Zouboulis, *Desalin. Water Treat.* **2013**, *51*, 2915.
- [7] a) Y. Xu, J. Zondlo, H. Finklea, A. Brennstainer, *Fuel Process. Technol.* **2000**, *68*, 189; b) L. Wang, R. Zhao, Z.-j. Gu, Y.-l. Zhao, Z.-f. Chai, W.-q. Shi, *Eur. J. Inorg. Chem.* **2014**, *2014*, 1158; c) C. Liu, P.-C. Hsu, J. Xie, J. Zhao, T. Wu, H. Wang, W. Liu, J. Zhang, S. Chu, Y. Cui, *Nat. Energy* **2017**, *2*, 17007.
- [8] C. Wang, T. Wang, J. Liu, Y. Zhou, D. Yu, J.-K. Cheng, F. Han, Q. Li, J. Chen, Y. Huang, *Energy Environ. Sci.* **2018**, *11*, 2467.
- [9] S. Drewniak, R. Muzyka, A. Stolarczyk, T. Pustelny, M. Kotyczka-Morańska, M. Setkiewicz, *Sensors* **2016**, *16*, 103.
- [10] J. Ederer, P. Janoš, P. Ecorchard, J. Tolasz, V. Štengl, H. Beneš, M. Perchacz, O. Pop-Georgievski, *RSC Adv.* **2017**, *7*, 12464.
- [11] a) J. Porwal, N. Karanwal, S. Kaul, S. L. Jain, *New J. Chem.* **2016**, *40*, 1547; b) A. Navae, A. Salimi, *RSC Adv.* **2015**, *5*, 59874.
- [12] Y. Zhang, Z. Sun, H. Wang, Y. Wang, M. Liang, S. Xue, *RSC Adv.* **2015**, *5*, 10430.
- [13] Z. Huang, Z. Li, L. Zheng, L. Zhou, Z. Chai, X. Wang, W. Shi, *Chem. Eng. J.* **2017**, *328*, 1066.

- [14] M. Patel, W. Feng, K. Savaram, M. R. Khoshi, R. Huang, J. Sun, E. Rabie, C. Flach, R. Mendelsohn, E. Garfunkel, H. He, *Small* **2015**, *11*, 3358.
- [15] a) D. Yang, A. Velamakanni, G. Bozoklu, S. Park, M. Stoller, R. D. Piner, S. Stankovich, I. Jung, D. A. Field, C. A. Ventrice, R. S. Ruoff, *Carbon* **2009**, *47*, 145; b) T. Lin, F. Huang, J. Liang, Y. Wang, *Energy Environ. Sci.* **2011**, *4*, 862.
- [16] a) H. Wang, H. Guo, N. Zhang, Z. Chen, B. Hu, X. Wang, *Environ. Sci. Technol.* **2019**, *53*, 6454; b) X. Liu, H. Pang, X. Liu, Q. Li, N. Zhang, L. Mao, M. Qiu, B. Hu, H. Yang, X. Wang, *Innovation* **2021**, *2*, 100076.
- [17] K. Müller, V. Brendler, H. Foerstendorf, *Inorg. Chem.* **2008**, *47*, 10127.
- [18] a) A. Yang, Y. Zhu, C. P. Huang, *Sci. Rep.* **2018**, *8*, 9058; b) J. L. Vivero-Escoto, M. Carboni, C. W. Abney, K. E. deKrafft, W. Lin, *Microporous Mesoporous Mater.* **2013**, *180*, 22; c) M. Carboni, C. W. Abney, S. Liu, W. Lin, *Chem. Sci.* **2013**, *4*, 2396; d) Z. Bai, L. Yuan, L. Zhu, Z. Liu, S. Chu, L. Zheng, J. Zhang, Z. Chai, W. Shi, *J. Mater. Chem. A* **2015**, *3*, 525; e) X. Hu, Y. Wang, J. O. Yang, Y. Li, P. Wu, H. Zhang, D. Yuan, Y. Liu, Z. Wu, Z. Liu, *Front. Chem. Sci. Eng.* **2020**, *14*, 1029.
- [19] a) Y. A. Teterin, V. M. Kulakov, A. S. Baev, N. B. Nevzorov, I. V. Melnikov, V. A. Streltsov, L. G. Mashirov, D. N. Suglobov, A. G. Zelenkov, *Phys. Chem. Miner.* **1981**, *7*, 151; b) Y. A. Teterin, *J. Struct. Chem.* **1998**, *39*, 850; c) E. S. Ilton, P. S. Bagus, *Surf. Interface Anal.* **2011**, *43*, 1549.
- [20] A. M. Deane, *J. Inorg. Nucl. Chem.* **1961**, *21*, 238.
- [21] R. L. Frost, J. Čejka, M. Weier, W. N. Martens, *J. Raman Spectrosc.* **2006**, *37*, 879.
- [22] M. L. Palacios, S. H. Taylor, *Appl. Spectrosc.* **2000**, *54*, 1372.
- [23] M. Pradhan, S. Sarkar, A. K. Sinha, M. Basu, T. Pal, *CrystEngComm* **2011**, *13*, 2878.
- [24] a) L. Andrews, X. Wang, Y. Gong, G. P. Kushto, B. Vlaisavljevich, L. Gagliardi, *J. Phys. Chem. A* **2014**, *118*, 5289; b) R. D. Hunt, J. T. Yustein, L. Andrews, *J. Chem. Phys.* **1993**, *98*, 6070.
- [25] S. Ahrland, S. Hietanen, L. G. Sillén, *Acta Chem. Scand.* **1954**, *8*, 1907.
- [26] S. Manna, S. B. Roy, J. B. Joshi, *J. Nucl. Mater.* **2012**, *424*, 94.
- [27] V. J. Wheeler, R. M. Dell, E. Wait, *J. Inorg. Nucl. Chem.* **1964**, *26*, 1829.
- [28] a) A. M. Saliba-Silva, R. H. L. Garcia, E. Bertin, E. F. Urano de Carvalho, M. Durazzo, *ECS Trans.* **2013**, *45*, 5; b) A. M. Saliba-Silva, E. T. de Oliveira, M. Durazzo, *ECS Trans.* **2014**, *61*, <https://doi.org/10.1149/06124.0001ecst>; c) W. Parker, H. Bildstein, N. Getoff, *Nature* **1963**, *200*, 457.
- [29] C. Wang, X. Wang, Y. Wang, J. Chen, H. Zhou, Y. Huang, *Nano Energy* **2015**, *11*, 678.
- [30] J. P. Perdew, K. Burke, M. Ernzerhof, *Phys. Rev. Lett.* **1997**, *78*, 1396.
- [31] P. E. Blöchl, *Phys. Rev. B* **1994**, *50*, 17953.
- [32] H. J. Monkhorst, J. D. Pack, *Phys. Rev. B* **1976**, *13*, 5188.
- [33] S. Grimme, J. Antony, S. Ehrlich, H. Krieg, *J. Chem. Phys.* **2010**, *132*, 154104.

ADVANCED MATERIALS

Supporting Information

for *Adv. Mater.*, DOI: 10.1002/adma.202102633

Uranium In Situ Electrolytic Deposition with a Reusable
Functional Graphene-Foam Electrode

Chao Wang, Ahmed S. Helal, Ziqiang Wang, Jian Zhou,
Xiahui Yao, Zhe Shi, Yang Ren, Jinhyuk Lee, Jeng-Kuei
Chang, Bunshi Fugetsu, and Ju Li**

Supporting Information

Uranium In-situ Electrolytic Deposition with a Reusable Functional Graphene-Foam Electrode

Chao Wang,* Ahmed S. Helal, Ziqiang Wang, Jian Zhou, Xiahui Yao, Zhe Shi, Yang Ren, Jinhyuk Lee, Jeng-Kuei Chang, Bunshi Fugetsu, Ju Li*

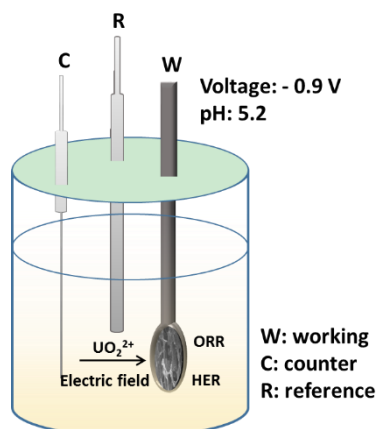


Figure S1. Schematic of the three-electrode setup for uranium electrochemical extraction. The reactions on working electrode are: $2\text{H}_2\text{O} + \text{O}_2 + 4\text{e}^- \rightarrow 4\text{OH}^-$ and $2\text{H}_2\text{O} + 2\text{e}^- \rightarrow \text{H}_2 + 2\text{OH}^-$.



Figure S2. Photograph of the 3D-FrGOF foam before and after press.

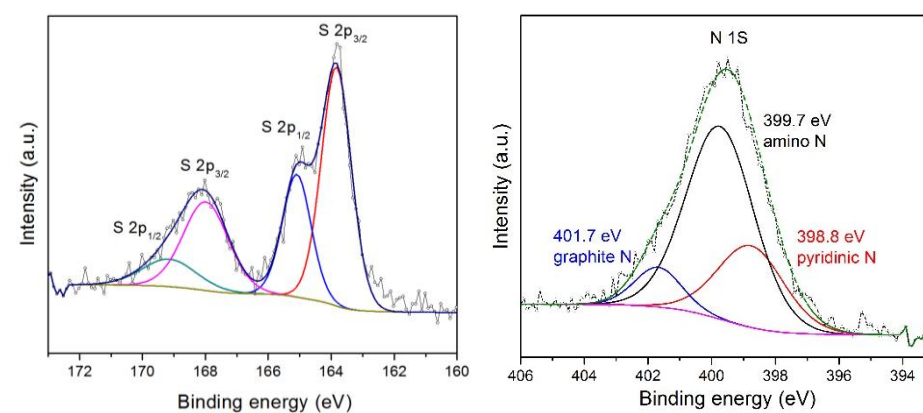


Figure S3. XPS spectra of N and S of the 3D-FrGOF.

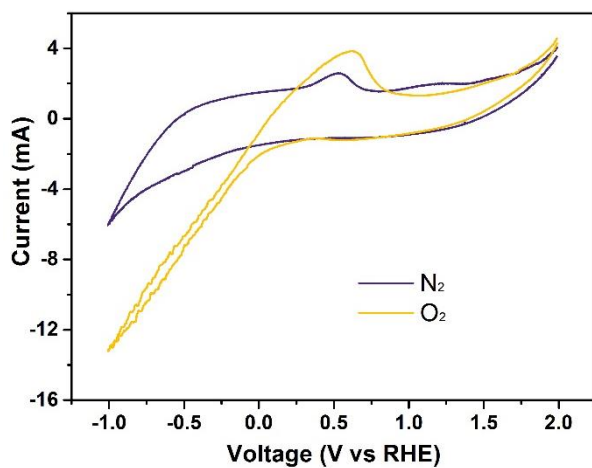


Figure S4. CV of the 3D-FrGOF under different conditions without uranium.

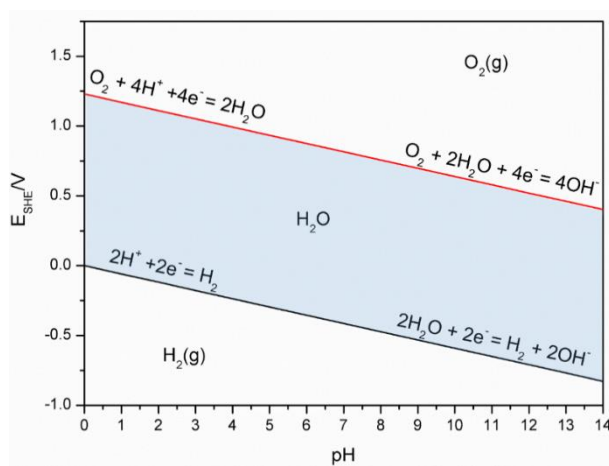


Figure S5. Pourbaix diagram of water.

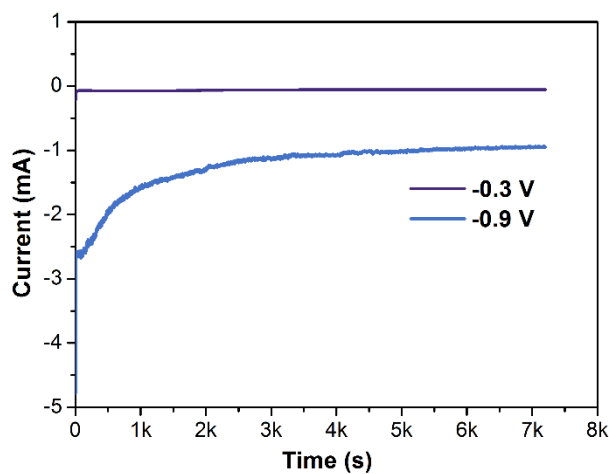


Figure S6. Current change during constant voltage applied at -0.3 and -0.9 V.

Solid phase extraction experiment were done in uranium solution. 3D-FrGOF was grounded into powder and then dispersed into uranium contaminated solution by sonicate. Then the solution was shake for 3 h. After that, the solution is separated from the powder by vacuum filter and the remained uranium is checked by ICP-OES

Table S1. Comparison of several uranium extraction methods

Method	Materials	Performance	Comment	Ref.
Chemical absorption	Polysulfide/Layered Double Hydroxide	pH 4, 10-600 ppm U, 24h, 330 mg/g	slow adsorption rate, unstable in acidic medium	S1
	Functionalized magnetic nanocomposite	pH 6, 100 ppm U, 2h, 286 mg/g 10 cycles	low sorption capacity, leaching of magnetic core	S2
	2D amidoxime-functionalized COFs	pH 6, 23.1-265.2 ppm U, saturated capacity 408 mg/g 3 cycles	Complex synthesis, expensive	S3
Electro-coagulation	Al-stainless steel Fe-stainless steel anode/cathode	70mA/cm ² , 2h, 0.126 mg/g	poor selectivity, consume electrode, further separation need	S4
	iron anode+ grahite cathode+ organic ligand	pH 6.0, i= 0.6 mA/cm ² , organic ligand to U(VI) = 3:1		S5
Electro-chemical method	Functionalized MXene electrode	pH 5, 200 ppm U, 12h, -0.7V, 626 mg/g	unstable in acidic medium	S6
	Phosphate-functionalized graphene hydrogel	pH 5, 100 ppm U, 1h, 1.2V, 545.7 mg/g 6 cycle	Work as CDI, lack of selectivity	S7
Membranes	SβCD based DA-PAN membrane	pH 7, 60 min, saturated capacity 378.8 mg/g 10 cycles	Expensive, initial stage, complex preparation	S8
	Di(2-ethylhexyl) phosphoric acid/PVC	100 mg/L in 0.1M H ₂ SO ₄ , pH 2, 50 h, 5 cycles	Poor durability, slow transport rate	S9
HW-ACE	Carbon cloth-PANI	1000mg/L, 1932 mg/g -5V, 400Hz, 12h 3 cycles	Long operation time Elute to 0.1 M HCl	S10
Our work	Sulfur and nitrogen functionalized 3D graphene foam	600mg/L, 4560 mg/g, -0.9V, 2h 10 cycles	Elute to 2000mg/L, 54% Coulombic efficiency	Our work

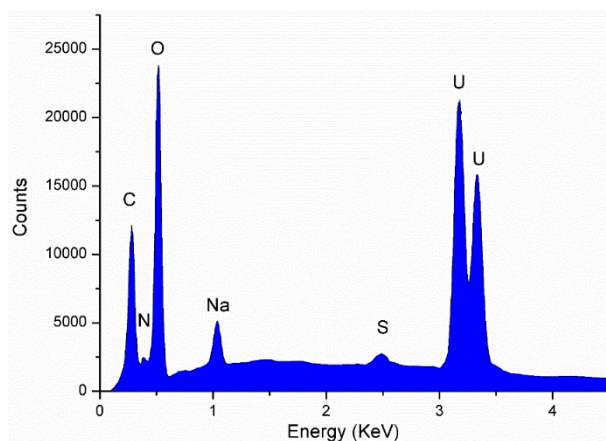


Figure S7. Energy spectrum of the 3D-FrGOF electrode after uranium precipitate.

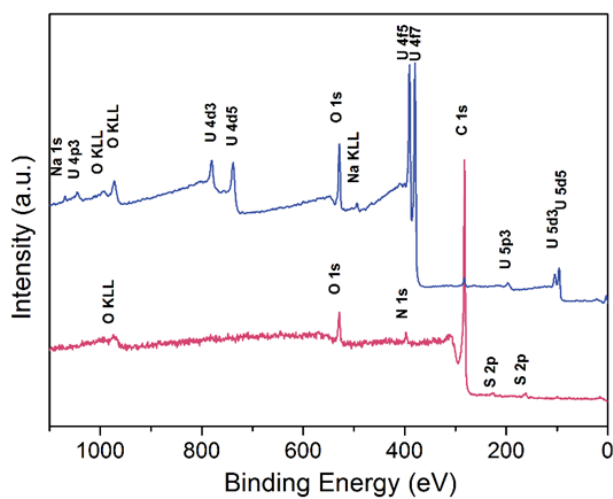


Figure S8. XPS spectra survey of the 3D-FrGOF electrode before and after uranium precipitation.

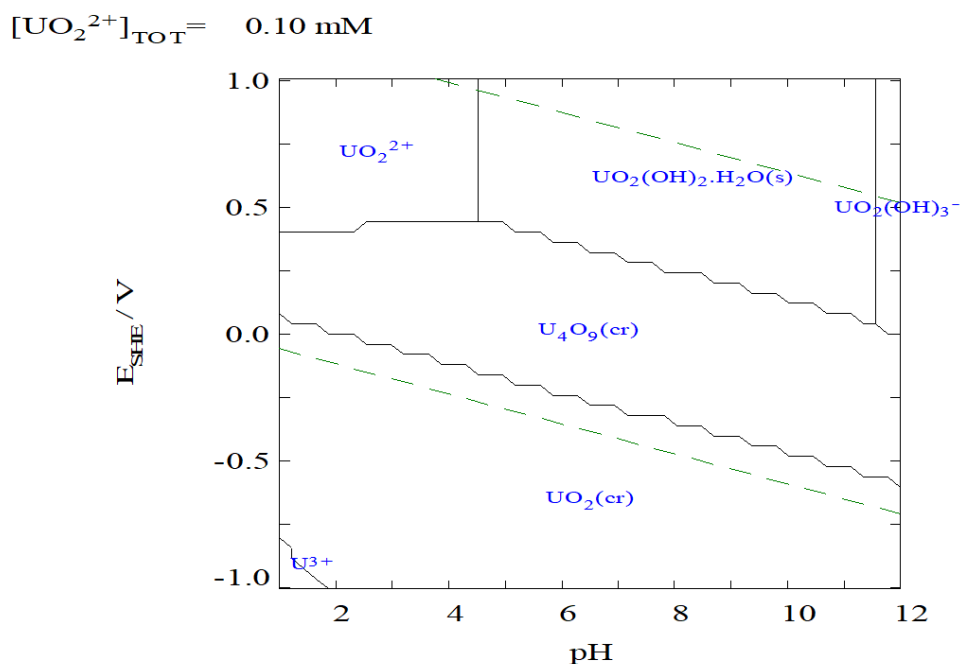


Figure S9. Pourbaix diagram of uranium with a uranium concentration of 0.1mM (~24ppm). The Eh-Ph diagram was calculated by Hydra-Medusa.

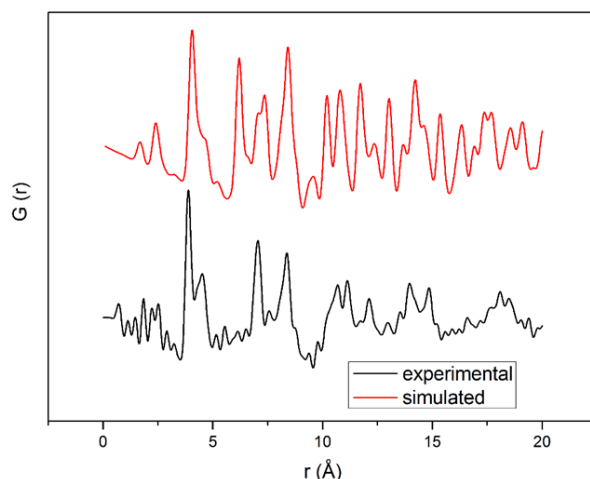


Fig. S10, Experimental and simulated pair distribution function curves of the precipitation.

Reference

- [S1] S. Ma, L. Huang, L. Ma, Y. Shim, S. M. Islam, P. Wang, L.-D. Zhao, S. Wang, G. Sun, X. Yang, M. G. Kanatzidis, *Journal of the American Chemical Society* 2015, 137, 3670.
- [S2] A. S. Helal, E. Mazario, A. Mayoral, P. Decorse, R. Losno, C. Lion, S. Ammar, M. Hémadi, *Environmental Science: Nano* 2018, 5, 158.
- [S3] Q. Sun, B. Aguila, L. D. Earl, C. W. Abney, L. Wojtas, P. K. Thallapally, S. Ma, *Advanced Materials* 2018, 30, 1705479.
- [S4] E. Nariyan, M. Sillanpää, C. Wolkersdorfer, *Separation and Purification Technology* 2018, 193, 386.
- [S5] P. Li, B. Zhun, X. Wang, P. Liao, G. Wang, L. Wang, Y. Guo, W. Zhang, *Environmental Science & Technology* 2017, 51, 14368.

- [S6] P. Zhang, L. Wang, Z. Huang, J. Yu, Z. Li, H. Deng, T. Yin, L. Yuan, J. K. Gibson, L. Mei, L. Zheng, H. Wang, Z. Chai, W. Shi, *ACS Applied Materials & Interfaces* 2020, 12, 15579.
- [S7] Y. Liao, M. Wang, D. Chen, *Applied Surface Science* 2019, 484, 83.
- [S8] N. Li, L. Yang, X. Ji, J. Ren, B. Gao, W. Deng, Z. Wang, *Environmental Science: Nano* 2020, 7, 3124.
- [S9] A. M. St John, R. W. Cattrall, S. D. Kolev, *Journal of Membrane Science* 2012, 409-410, 242.
- [S10] C. Liu, P.-C. Hsu, J. Xie, J. Zhao, T. Wu, H. Wang, W. Liu, J. Zhang, S. Chu, Y. Cui, *Nat Energy* 2017, 2, 17007.